Journal of Sound and Vibration 357 (2015) 35–50

Contents lists available at ScienceDirect

Journal of Sound and Vibration

journal homepage: www.elsevier.com/locate/jsvi

On the efficiency and robustness of damping by branching

Benoit Théckès [a,1], Xavier Boutillon [b,*], Emmanuel de Langre [a]

[a] LadHyX, CNRS - École Polytechnique, F-91128 Palaiseau, France
[b] LMS, CNRS - École Polytechnique, F-91128 Palaiseau, France

ARTICLE INFO

Article history:
Received 9 July 2014
Received in revised form
30 June 2015
Accepted 18 July 2015
Handling Editor: Ivana Kovacic
Available online 14 August 2015

ABSTRACT

This paper investigates the mechanism referred to as damping by branching (DBB), and its ability to attenuate the response of an oscillating structure, in the range of large amplitudes. More specifically, we give an experimental proof of this mechanism and we show that it is very robust against variations of the physical parameters and constituents: nature of the damping mechanism, geometrical structure. These results motivated the design of the Tuned Mass Branched Damper (TMBD) which is shown to be a little more efficient than the classical Tuned Mass Damper (TMD) in some domains of the parameter space.

1. Introduction

Damping by branching (DBB) was identified recently by [1] as a simple mean to damp an oscillating beam, referred to as the trunk, by means of the oscillations of beams attached to it, the branches. Damping of vibration in trees originates in wood viscoelasticity and in interactions with air [2,3]. Yet, significant exchange of energy between parts of the trees are known to play an important role in the damping of large amplitude motions [4–10]. Essentially, the mechanism responsible for the damping of the trunk mode is the transfer of energy to the branches, through geometrical nonlinearities, followed by the dissipation in the motion of the branches. This was elucidated using the simple lumped parameter model shown in Fig. 1 with two degrees of freedom. The 2:1 resonance between the branch and the trunk mode was shown to bring an effective damping of up to 3 percent for a damping of about 20 percent in the branches (see [1]: effective damping of ≈ 1.8 percent in Fig. 5b for $E_0 = 1$ with the lumped parameter model and of ≈ 3 percent in Fig. 7 for $E_0 \approx 1$ with the continuous model). By Finite Element computation of more complex branched systems made of flexural beams, it was shown that the mechanism is also efficient in the presence of a large number of modes.

Although the concept of DBB seems promising, many questions remain as to its applicability in designing efficient dampers. First, this type of damping has never been evidenced experimentally although some observations on trees [11] suggest that it does exist. Second, the robustness of the effect was not studied in [1]. Third, DBB needs to be evaluated in comparison with other damping methods.

The purpose of the present paper is to answer these questions. In Section 2, we recall the main features of the DBB mechanism. Experimental results are shown in Section 3 and compared to those obtained with the simplistic model presented in Section 2. The robustness of the mechanism is explored in Section 4, and a comparison is presented in Section 5

* Corresponding author.

[1] Present address: 18 rue du stade, F-29290 Saint Renan, France.

http://dx.doi.org/10.1016/j.jsv.2015.07.018
0022-460X/

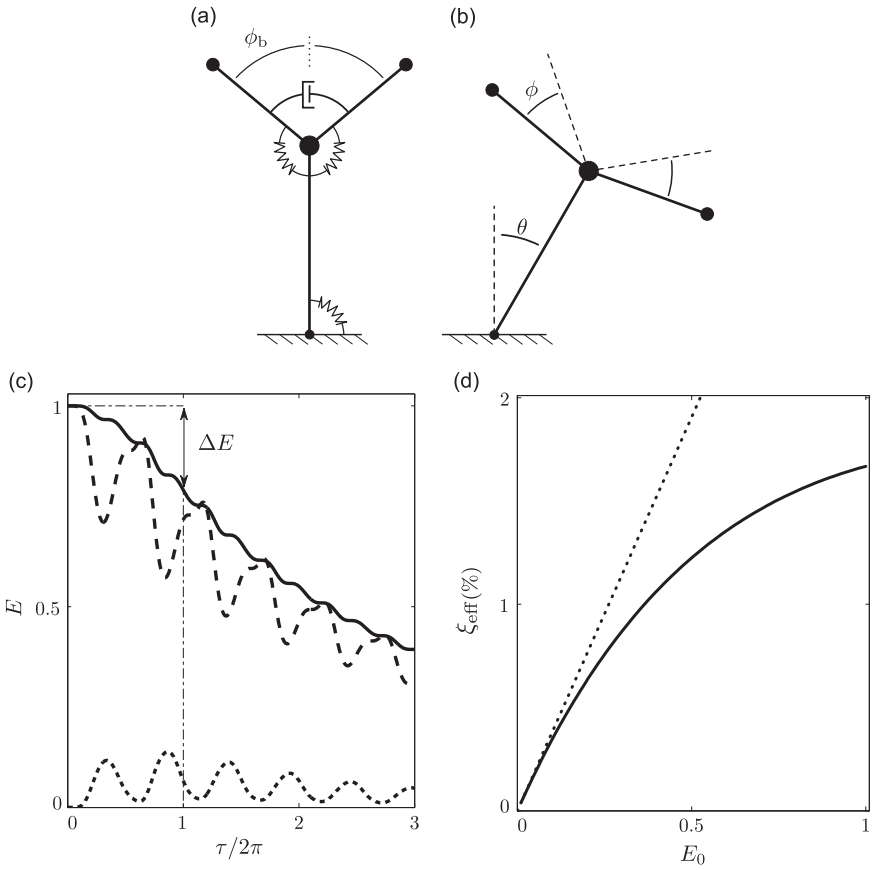

Fig. 1. Lumped-element model used in [1] to study DBB. (a) Geometry of the branched system. (b) Motion involving two degrees of freedom θ and ϕ. (c) Decay of the normalised energies in the system after an initial displacement of the trunk mode only (see text for the choice of normalisation). Solid line ——: total energy. Dashed line (– –): energy in the trunk mode. Dotted line (·····): energy in the branch mode. (d) Effective damping ξ_{eff} of the system as a function of the initial energy E_0 (from [1], (4)). Dashed line (– –): analytical solution for low motion amplitude (see Eq. (3)). Solid line (——): general case. The parameters of the structure correspond to optimal damping: $\phi_b = \pi/2, \xi_b = 0.2\%, \Gamma = 0.2$.

between the classical Tuned-Mass Damper (TMD) and one implementation of the DBB effect. The main results and effects are recalled in the concluding remarks.

2. Main features of damping by branching

We recall here the main features of DBB, as defined in [1], using the elementary model shown in Fig. 1. The model is based on the motion of three rigid bars linked by rotational springs and supporting three masses. The first bar, referred to as the trunk, has a length ℓ_1, is linked to the ground by a rotational spring k_1 and supports a mass m_1. Its motion is defined by the angle θ. The branches are two symmetrical bars of length ℓ_2, each originally forming an angle ϕ_b with respect to the axis of the trunk. Each branch is linked to the tip of the trunk by a rotational spring k_2, and supports a mass m_2. A dissipative element c_b is introduced between the branches. We consider only their symmetrical motion defined by the angle ϕ. In the limit of small motion, the first mode (trunk mode) involves θ only and the second mode (branch mode) ϕ only. The corresponding dimensionless equations of motion have been derived in [1]:

$$\ddot{\Theta}+\Theta = 2\Gamma\left[\dot{\Theta}\dot{\Phi}\sin(\phi_b+\Phi)-\ddot{\Theta}\left(\cos(\phi_b+\Phi)-\cos\phi_b\right)\right]\quad \ddot{\Phi}+2\Omega\xi_b\dot{\Phi}+\Omega^2\Phi = -\dot{\Theta}^2\sin(\phi_b+\Phi) \tag{1}$$

where ξ_b is the damping ratio of the branch mode, Ω is the ratio between the frequencies of the trunk and branch modes, Γ is a mass ratio, Θ and Φ are rescaled angles, time derivation is with respect to the normalised time τ (see Appendix A for the definition of dimensionless quantities).

By analysing the free response of the system to an initial condition imposed on Θ only, it appears that the amplitude of this mode decreases through transfer to the branch mode. The resulting effective damping of the trunk mode ξ_{eff} is defined as

$$\xi_{\text{eff}} = \frac{\Delta E}{4\pi E_0} \tag{2}$$

where ΔE is the energy lost after one period of the trunk mode and E_0 is the initial energy of the system (symbols refer here to normalised energies defined below). The evolution of this energy is shown in Fig. 1. It is found that the effective damping depends on the amplitude of motion. After normalisation of the energies so that $E_0 = 1$ for $\Theta = \pi/2$ and $\dot{\Theta} = 0$, a first-order approximation gives

$$\xi_{\text{eff}} = E_0 \Gamma \ \sin^2 \phi_b \ \overline{\xi}(\xi_b, \Omega). \tag{3}$$

The function $\overline{\xi}(\xi_b, \Omega)$ (see [1], Fig. 2) has a maximum near $\Omega = 2$ (2:1 resonance) and $\xi_b = 0.2$ (optimal damping). In fact, the 2:1 resonance is optimal in order to excite the branch mode by the motion of the trunk, as can be seen in Eq. (1) where the branch mode is excited at twice the frequency of the oscillation of the trunk. The existence of an optimal damping to put on the branch may be understood as follows: for low damping, the dissipation in the branch is not sufficient and most of the energy is transferred back to the trunk mode, resulting in low effective damping. Conversely, for high branch damping the motion of branches remains small, resulting in a low effective damping. Between these two extreme cases, a maximum can be found. The effective damping is also proportional to the mass ratio Γ. Finally, it can be seen in Eq. (3) that the optimal angle of branching is $\phi_b = \pi/2$, where the branches are orthogonal to the trunk. It was shown numerically that these optimal values yield also optimal effective damping for large amplitude motions. The E_0-dependency of ξ_{eff} is represented in Fig. 1(d). The complete results for the parameter-dependency of ξ_{eff} have also been given in [1] and are shown here in Fig. 7 (case $n = 1$).

3. Experimental evidence

One experimental counterpart of the model presented in the previous section is shown in Fig. 2. The trunk and the branches are made of two PVC strips that are clamped respectively in the support and on the trunk. The large ratio (30) between the thickness and the width of the strips and the "T" arrangement where the length of the branch is along the width of the trunk (instead of the thickness) guarantees that the first two modes (Fig. 3) have much lower frequencies than all other ones. The value of the small masses added near the end of each branch and the quantity of rubber-band glued at the trunk-branches junction are adjusted so that $\Omega = 2$ and $\xi_b \approx 13$ percent respectively. The damping coefficient ξ_b has been measured in a test where the trunk is blocked, the branches vibrate freely (see the definition of ξ_b after Eq. (1)) and the logarithmic decrement of the vibration (sensor described below) is evaluated. Once the geometry and masses of the structure are chosen, the modal masses m_1 and m_2 are evaluated, yielding the value of Γ to be ≈ 0.22, in the same range as in the numerical experiments presented all along this paper (the case of the continuous elementary branched structure is treated in Section 3.1 of [1], yielding $\Gamma = (l_1 m_2)/(l_2 m_1)$).

The trunk is deflected by a nylon thread which is burnt to obtain a motion with zero initial velocities. Given its geometry (a flat beam), it can be deflected in only one direction in practice. The horizontal component of its motion, denoted by $X(t)$, is measured at about a quarter of its height (thus remaining very close to the deflection, even for large motions) by a laser sensor (Keyence LB-70W) and digitised at 500 Hz, giving about 250 points per period of the trunk mode. Since the motion of the branches proved difficult to measure reliably when the trunk is vibrating, the effective damping is defined by the

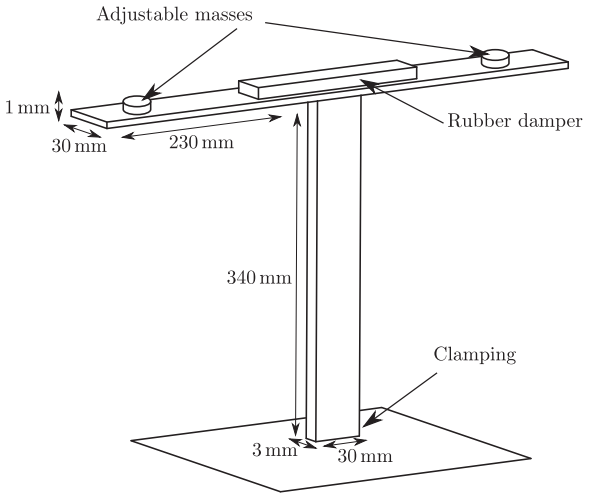

Fig. 2. Schematic view of a branched structure. Damping and frequencies are adjusted by means of the rubber damper and the adjustable masses. This variant of a symmetrical "T" assembly is such that the branches and the trunk do not vibrate in the same plane, ensuring practically that the dynamics are restricted to two modes only.

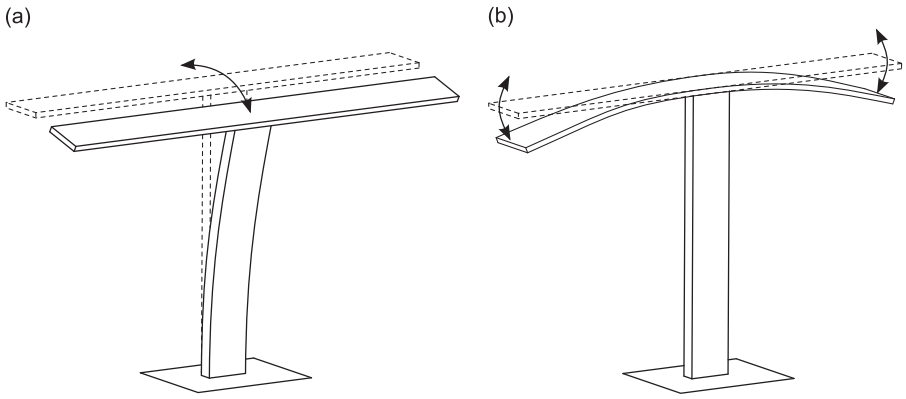

Fig. 3. (a) Trunk mode. (b) Branch mode. All other modes have much higher frequencies.

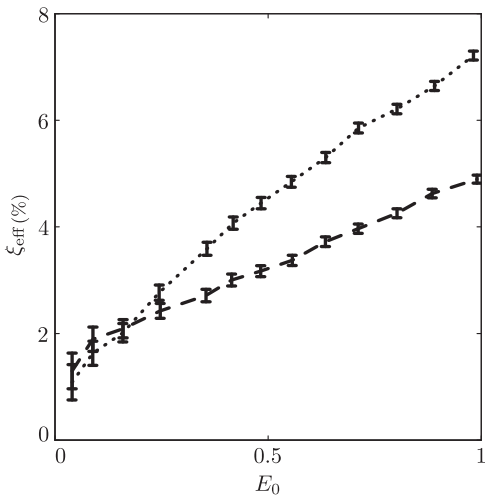

Fig. 4. Measured effective damping ξ_{eff} as a function of the initial energy E_0 (static initial condition). Dotted (·····): free branches. Dashed (– –): blocked branches.

logarithmic decrement of the trunk deflection only, such that

$$\xi_{\text{eff}} = \frac{1}{2\pi}\log\frac{X_0}{X_1}, \tag{4}$$

where $X_0 = X(0)$ is the initial deflection, and X_1 is the deflection after one free oscillation of the trunk mode. The initial energy of the trunk X_0^2 is now normalised to its value when the initial deflection of the trunk at its top is equal to its height. The quantitative analysis done in [1] and based on the curves shown in Fig. 1(c) prove that, for the values of the parameters chosen here, most of the energy is located in the trunk. Finally, the higher modes of the trunk are very weakly excited in this experiment. Altogether, the error made on ξ_{eff} by restricting the estimation of energy to the trunk is very small.

We are interested in the specific dynamical effect of branching on damping, denoted here as ξ_{DBB}. In any experimental situation, other dissipative effects occur which may also be difficult to control. For this reason, we compare damping when branches are free to vibrate to damping when the branches are blocked by a very light flat beam taped across the branches: in Fig. 4, the effective damping is displayed as a function of the initial energy, for blocked and free branches. For blocked branches, damping is nonlinear, probably because of aerodynamical effects. Its finite value for $E_0 \to 0$ (linear part) most probably denotes dissipation in the material. It is clear that DBB becomes an important part of the effective damping ξ_{eff} for large motions. We assume that (a) the other-than-DBB effects are the same whether branches are free or blocked (this is not entirely true: for example, aerodynamical effects are slightly increased when branches vibrate on their own) and (b) that the effective damping ξ_{efff} with free branches is the *sum* of ξ_{DBB} and damping observed with blocked branches. The ξ_{DBB}-component (difference between curves in Fig. 4) is displayed in Fig. 5 together with the effective damping of the lumped-element model (Section 2) and the damping obtained in the case of a T-shape beam structure. Unlike the former, the latter is fully deformable and its response has been obtained by finite-elements numerical computation [1].

We attribute the negative values of ξ_{DBB} at very small amplitudes, where the effect is virtually null, to uncertainties in the estimation of the effective damping, mostly due to the sensor measuring the motion of the trunk. Damping by branching is

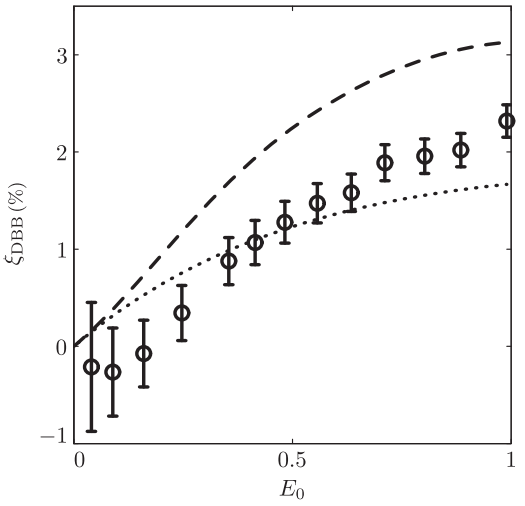

Fig. 5. Damping by branching component ξ_{DBB} (○ symbols with error bars) in the measured effective damping ξ_{eff} of the structure with free branches (Fig. 4) as a function of the initial energy (static initial conditions). Comparison with the effective dampings of the lumped-element model (· · · · · ·) and of a similar T-shape beam structure (– – –), as shown respectively in Figs. 4 and 7 of [1].

effective for large amplitudes and its estimated magnitude is quite consistent with (and actually framed by) the models that can be considered as idealisations of the experimental structures.

4. Robustness of the mechanism

In the previous sections, DBB has been presented for free-vibrating structures. A first indication of the robustness of the mechanism has been demonstrated in [1] where it was shown that a branched assembly of flexible beams under harmonic excitation exhibits DBB as well as the lumped-element model: ξ_{eff} is in the order of 3 percent (see dashed line in Fig. 5) for an excitation of the trunk mode corresponding to $E_0 = 1$.

4.1. Nonlinear localised damping

We show here that the main features of DBB remain when the linear damping term $2\Omega\xi_b\dot{\Phi}$ of the branch mode in Eq. (1) is replaced by a nonlinear damping term $2\Omega\xi_b\dot{\Phi}|\dot{\Phi}|^{n-1}$. For reasons given above, it is difficult to isolate one of these damping models experimentally. However, the first two forms reflect common damping situations ($n=0$: damping by Coulomb friction, $n=1$: viscous damping, $n=2$: aerodynamical damping) and the successive powers n encompass a large variety of situations. Further on, intuition would be severely defeated if DBB was not robust at least to any monotonic form of damping whereas it is robust for the n-series, as shown below. The analyses are done on the lumped-element model described in Section 2.

In the case of small motion, a semi-analytical solution for the effective damping $\xi_{\mathrm{eff}} = \Delta E/(4\pi E_0)$ can be obtained by a harmonic balance method [12], as in [1] (see details in [13]). All calculations are done with a linear part (order 1) and a nonlinear part limited to order 2 (in other words, the harmonic balance method takes into account only two harmonics). For $n \geq 2$, it comes

$$\dot{\Phi} = \frac{-\Omega \sin 2\tau + 2\sin \Omega\tau}{\Omega(\Omega^2 - 4)} \tag{5}$$

$$\overline{\xi}_n(\Omega) = \frac{2\pi^{2n-1}}{4^{n+1}} \int_0^{2\pi} 2\Omega\dot{\Phi}^2 |\dot{\Phi}|^{n-1}\, \mathrm{d}\tau \tag{6}$$

$$\xi_{\mathrm{eff}} = E_0^n\, \Gamma\, (\sin\phi_b)^{n+1}\, \xi_b\, \overline{\xi}_n(\Omega) \tag{7}$$

where the dimensionless variables Ω, τ, Φ, Γ are defined as in Appendix A.

The E_0^n dependency of ξ_{eff} corresponds to a $\dot{\Theta}^{2n+1}$ dependency of the effective damping force on the trunk mode. In other words, branching transfers damping from the branches to the trunk at the price of increasing the nonlinearity order of the damping. Linear damping in the branch mode ($n=1$, the largest damping in the case of small motion) yields an effective damping proportional to E_0. According to [12], this corresponds to a damping coefficient for the trunk mode of third order in $\dot{\Theta}$. Thus, DBB cannot be efficient for small amplitudes of the motion of the branches.

For large motion, the time-dependency of the energy after the initial loading in Θ is obtained by a numerical resolution of the system (1) where the nonlinear damping term is now $2\,\Omega\,\xi_b\,\dot{\Phi}\,|\dot{\Phi}|^{n-1}$. The effective damping is given in Fig. 6 as a

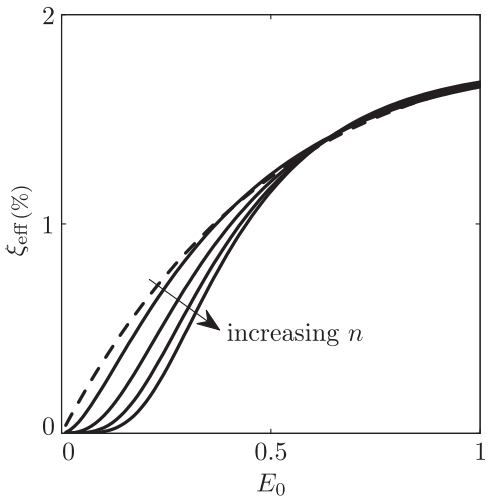

Fig. 6. Effective damping of the lumped-element branched model with nonlinear damping of the branch mode, as a function of the initial normalised energy. Solid lines (——): $n=2$, 3, 4 and 5. Dashed line (– – –): linear damping ($n=1$). The parameters of the structure are those given in [1] for optimal damping: $\phi_b=\pi/2$, $\xi_b=0.2\%$, with $\Gamma=0.2$.

function of the initial loading for several degrees n of the nonlinear damping. It appears that the effective damping at large amplitudes hardly depends on the order of the nonlinear damping of the branch mode. This robustness of DBB with regard to n is also observed with regard to the parameters ϕ_b, ξ_b, Ω and Γ (Fig. 7): their influence on ξ_{eff} appears to be essentially the same as for the linear damping ($n=1$).

4.2. Aerodynamical damping

In order to test further the robustness of DBB, we analyse the effect of the aerodynamical damping caused by a fluid at rest on the structure shown in Fig. 8. This more realistic damping mechanism applies to the branches *and* to the trunk. The velocity at a given point on a rod is noted as $\underline{V}$ and its component normal to the rod is $\underline{V_n}=\underline{V}-(\underline{V}\cdot\underline{s})$, with $\underline{s}$ being the unit vector in the beam direction (Fig. 8(b)). The drag force per unit length on beam i is modelled as

$$\underline{f_i}=-\tfrac{1}{2}\rho_f C_D d_i \underline{V_n}^{|2|} \tag{8}$$

where we denote the signed square function $x^{|2|}=x|x|$, d_i is the diameter of the beam i, ρ_f is the fluid density and C_D is the drag coefficient which we assume to be constant [3]. As in Section 2, the in-phase motion of the branches is not considered. One introduces the mass ratio [14] defined here as

$$\mathcal{M}=C_D\frac{\rho_f d_1 \ell_1^3}{4m_2\sqrt{\ell_1\ell_2}}. \tag{9}$$

The dimensionless equations of motion are now (see Appendix B for the definition of d and X and the derivation):

$$\ddot{\Theta}+\Theta=2\Gamma\Big(\dot{\Theta}\dot{\Phi}\sin(\phi_b+\Phi)-\ddot{\Theta}(\cos(\phi_b+\Phi)-\cos\phi_b)\Big)\frac{1}{4}\Gamma\mathcal{M}\dot{\Theta}^{|2|}-\Gamma\mathcal{M}d\Lambda\int_0^{\Lambda}\Big((\dot{\Theta}X+\dot{\Phi}x)^{|2|}$$
$$+(\dot{\Theta}X-\dot{\Phi}x)^{|2|}\Big)X\,\mathrm{d}x\ddot{\Phi}+\Omega^2\Phi=-\dot{\Theta}^2\sin(\phi_b+\Phi)-\mathcal{M}d\Lambda\int_0^{\Lambda}\Big((\dot{\Theta}X+\dot{\Phi}x)^{|2|}-(\dot{\Theta}X-\dot{\Phi}x)^{|2|}\Big)x\,\mathrm{d}x \tag{10}$$

In order to compare DBB with the case presented in Section 2, the same initial condition is considered ($\Theta_0\neq 0, \dot{\Theta}_0=\dot{\Phi}_0=\Phi_0=0$). However, the effective damping must be defined differently since the trunk mode is now damped even when the branch mode is blocked. We define the effective damping specific to DBB by comparison with the situation where the branch mode is blocked, for the same values of the parameters Ω, Γ, ϕ_b, Λ, d and $\mathcal{M}$. The dynamical equation of the trunk with blocked branches is derived from the first equation of (10) with $\dot{\Phi}=\Phi=0$, yielding

$$\ddot{\Psi}+\Psi=-\dot{\Psi}^{|2|}\Gamma\mathcal{M}\left(\frac{1}{4}+2\,d\Lambda\int_0^{\Lambda}\Big|x\Lambda+\cos\phi_b\Big|(x\Lambda+\cos\phi_b)^2\,\mathrm{d}x\right) \tag{11}$$

where Ψ denotes the motion of the trunk in this particular situation. The effective damping is now defined as

$$\xi_{\text{eff}}=\frac{E(\Psi,0,\dot{\Psi},0)-E(\Theta,\Phi,\dot{\Theta},\dot{\Phi})}{4\pi E_0} \tag{12}$$

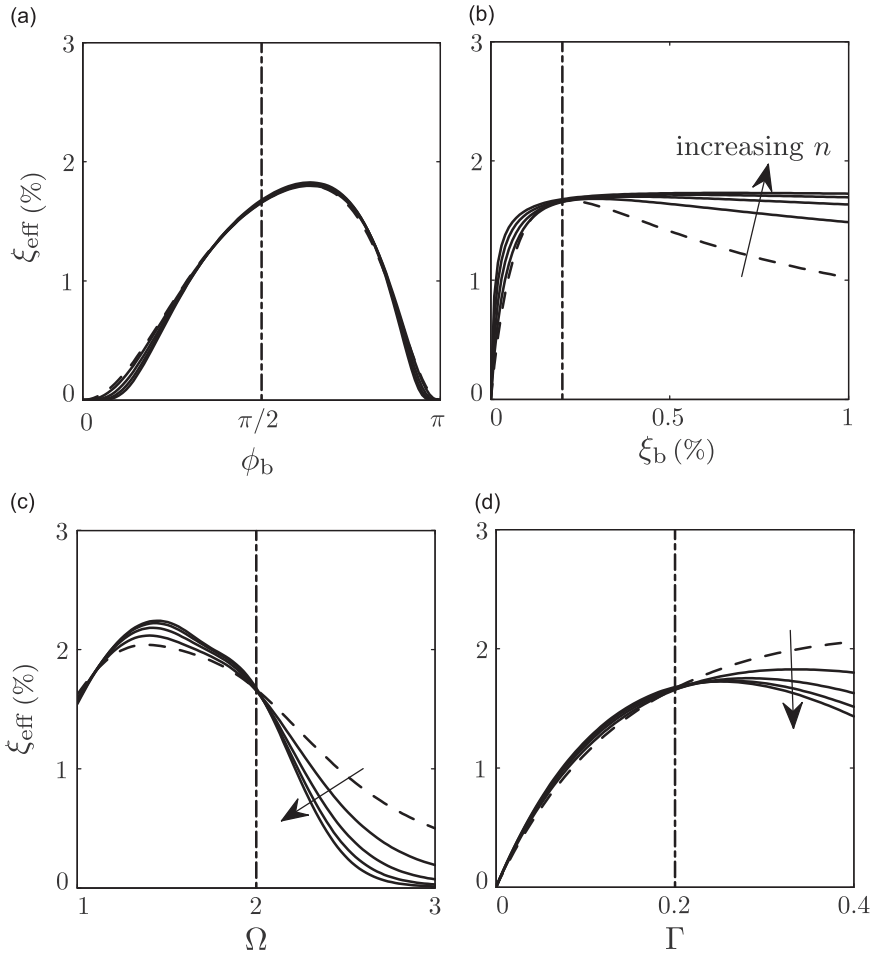

Fig. 7. Dependence of the effective damping ξ_{eff} on the parameters ϕ_b, ξ_b, Ω, Γ of the lumped-element branched model with initial normalised energy $E_0 = 1$. Solid lines (——): nonlinear damping of the branch mode with $n = 2, 3, 4, 5$. Dashed line (– – –): linear damping ($n = 1$). Non-varying parameters are set to the reference values given in Fig. 6 and indicated by a vertical dash-dotted line –· in the other diagrams. (a) Effect of the branching angle ϕ_b. (b) Effect of the damping of the branch mode ξ_b. (c) Effect of the ratio Ω between the frequency of the branch mode and that of the trunk mode. (d) Effect of the mass number Γ.

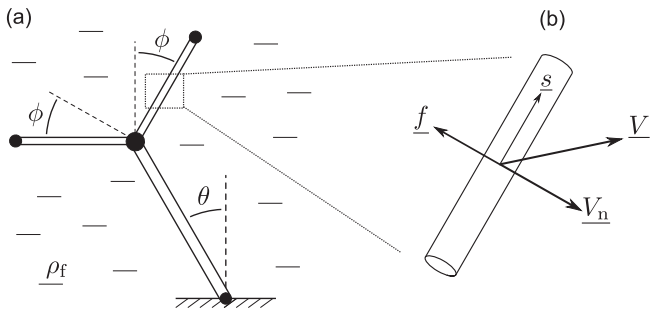

Fig. 8. Model for aerodynamical damping. (a) Elementary branched structure in a fluid at rest, similar to the model of Section 2, Fig. 1 (note here the relevance of the trunk and branch diameters d_1 and d_2). (b) Model of the aerodynamical forces exerted on a point of the left branch.

where energies in the numerator are evaluated at a normalised time $\tau = 2\pi$. It appears in Fig. 9 that DBB is observed in this situation, and that it is quantitatively very close to the linear damping of the branch mode. This robustness is confirmed by the dependency of ξ_{eff} on ϕ_b, $\mathcal{M}$, Ω, Γ, Λ and d (Fig. 10). The dependencies on ϕ_b, Ω and Γ appear again to be similar to what was shown in Fig. 7.

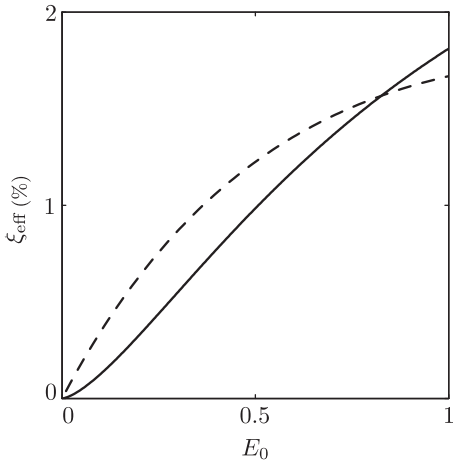

Fig. 9. Effective damping due to branching and aerodynamical distributed forces (see Eq. (12)) for the structure shown in Fig. 8, as a function of the initial normalised energy (solid ——). Dashed line (– – –): linear damping as in Section 2 or in Fig. 6 with $n=1$. Values of the parameters: $\Lambda=1$, $d=1/\sqrt{2}$, $\mathcal{M}=0.2$. The other parameters are those given in [1] for optimal damping: $\phi_b=\pi/2$, $\xi_b=0.2\%$ and $\Gamma=0.2$.

4.3. Multiple branching

At this point, one may wonder whether multiple branching significantly alters the efficiency of the DBB mechanism. Since the potential number of parameters increases dramatically with the number of ramifications, we restrict the attention to the branched structure obtained with a symmetrical self-similar branching scheme (Fig. 11) based on the reference model (Section 2, Fig. 1) where N is the number of ramification levels. As in Section 2, only the symmetrical motion of each branch level is considered, leaving only one mode, or effective degree of freedom, per branching level and $N+1$ degrees of freedom altogether. The same branching angle ϕ_b and damping ξ_b are kept at each branching level. The non-dimensional dynamical equations read (see Appendix C for the definition and expressions of Ω_n, Υ_n, $C_{n,k}$ and $H_{n,k}$ and for an outline of the derivation of the dynamical equations):

$$\ddot{\Phi}_n+2\Omega_n\xi_b\dot{\Phi}_n+\Omega_n^2\Phi_n=-\Upsilon_n\ddot{\Phi}_n+\dot{\Phi}_n\sum_{k=n+1}^{N+1}H_{n,k}\dot{\Phi}_k+\sum_{k=1}^{n-1}C_{n,k}\dot{\Phi}_k^2. \tag{13}$$

For reasons given after Eq. (C.13) in Appendix C, Ω_n cannot be expressed as a simple function of Ω.

Three additional choices are made in order to make the multiply branched model comparable with the elementary model: the overall branch mass, the mass ratio Γ_2 pertaining to the first branch level and the normalised frequency Ω_2 of the first branch mode are the same as the corresponding quantities of the elementary model (see the related equations (C.15)–(C.17)).

The coupling scheme for $N=2$ is presented in Fig. 12. At a given branching level n, nonlinear coupling terms with higher order modes are of the form $H_{n,k}\,\dot{\Phi}_n\,\dot{\Phi}_k$ whereas nonlinear coupling with lower order modes are in $C_{n,k}\dot{\Phi}_k^2$. Direct couplings appear between modes of orders i and j (with $i\neq j\pm1$). Due to the values of $C_{n,k}$ and $H_{n,k}$ (Eqs. (C.12) and (C.13)) they are more efficient than indirect couplings corresponding to a cascade path.

Again, a semi-analytical solution for small motions with initial energy on the trunk mode Φ_1 can be obtained by the harmonic balance method [12]. The effective damping is the result of energy dissipation at all the levels of branches:

$$\xi_{\text{eff}}(N)=E_0\sum_{n=2}^{N+1}\Gamma_n C_{n,1}^{\text{lin}2}\overline{\xi}(\Omega_n,\xi_b). \tag{14}$$

In this expression, Γ_n is given by Eq. (C.14), $E_0=(4/\pi^2)\Phi_1^2|_{\tau=0}$ is the initial energy and the $C_{n,1}^{\text{lin}}$ coefficients are the linear parts of the $C_{n,1}$ coefficients given by Eqs. (C.12) and (C.11). The $\overline{\xi}$ function has been introduced in Section 2. This result is an extension of Eq. (3) at N ramification levels.

For large amplitudes of motion, the dynamics is obtained by numerical integration of Eq. (13). The effective damping is presented in Fig. 13 and the parameter sensitivity in Fig. 14, for up to $N=4$ orders of branching.

Besides the robustness of DBB, it also appears that the convergence is very rapid with N. In this self-similar system, each level is damped by the upper level(s) and therefore, branches of the first level vibrate less than in the elementary model. This may explain why the effective damping is *less* for multiple branching than for simple branching, at least for these values of the parameters.

The relative insensitivity to the branching order can be explained by the fact that DBB is due to a 2:1 internal resonance and thus, is quite sensitive to Ω. Since Ω_n increases rapidly, it also departs rapidly from the optimal range, as far as direct couplings are concerned.

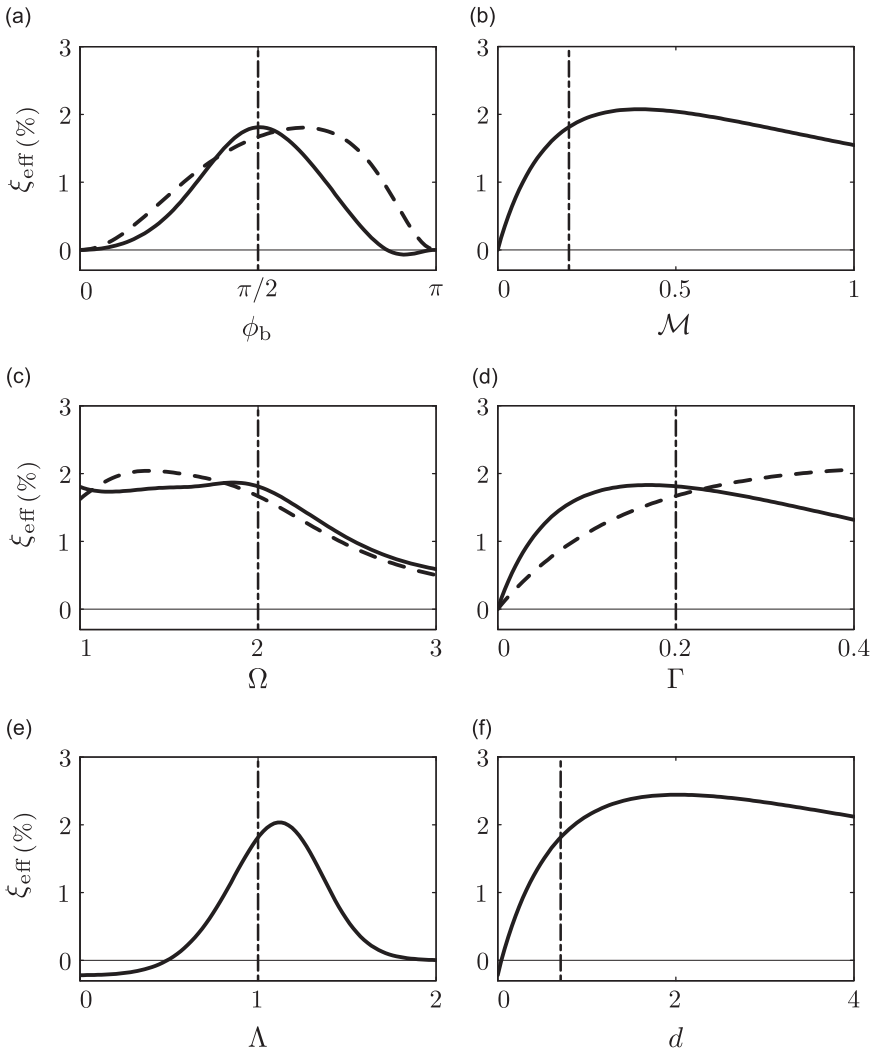

Fig. 10. Dependence of the effective damping ξ_{eff} as defined in Eq. (12) on the six parameters of the elementary structure (Fig. 8(a)). The initial normalised energy is $E_0 = 1$. Solid lines (——): aerodynamical damping. Dashed line (– – –): linear damping in the branch mode only. The values of the non-varying parameters are those given in Fig. 9 and indicated by a vertical dash-dotted line (– ·) in the other diagrams. (a) Effect of the branching angle ϕ_b. (b) Effect of the mass number $\mathcal{M}$. (c) Effect of the ratio Ω between the frequency of the branch mode and that of the trunk mode. (d) Effect of the mass number Γ. (e) Effect of the square root of the ratio of the branch and trunk lengths Λ. (f) Effect of the ratio of the branch and trunk diameters d.

As suggested by a reviewer of this paper, tuning the eigenfrequencies of the branches in a 1:2:4:8 series might increase the efficiency of the (overall) damping mechanism. Such a tuning would require that the relationships ruling the self-similar system be different from those given by Eq. (C.1). However, the above remark on the decreasing vibration level (with branching order) would presumably still limit the amount of attainable damping.

5. A Tuned Mass Branched Damper

Damping the vibrations of engineered structures (buildings, cars, etc.) can often be done with Tuned Mass Dampers (TMD) [15]: a damped spring–mass system, light compared to the mass of the main structure, is tuned to absorb energy in the vicinity of a frequency of interest. We propose to use DBB as the damping mechanism in a rotational TMD (Fig. 15): given the nonlinear character of DBB, this arrangement is expected to provide increasing damping when the amplitude of motion increases, which occurs naturally at resonance. We coin such a device as Tuned Mass *Branched* Damper (TMBD). Its damping performance are assessed below in comparison to an equivalent and optimal TMD design.

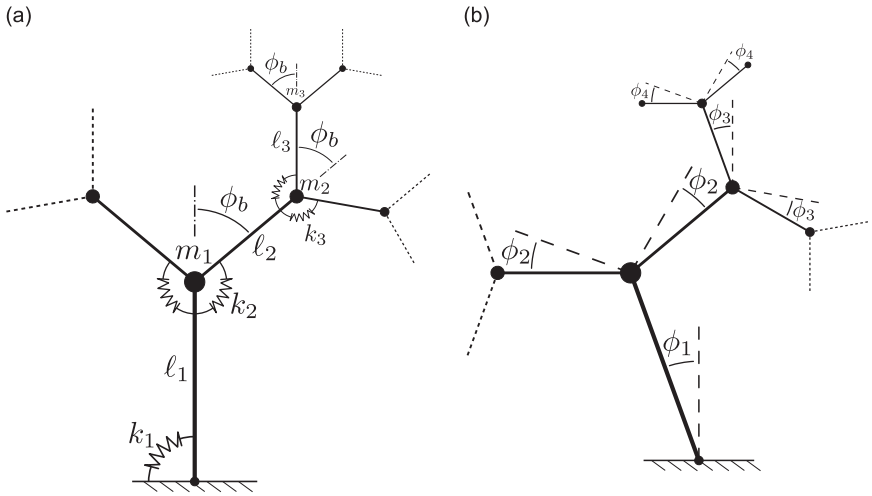

Fig. 11. Multiply branched structure: the elementary model shown in Fig. 1 is duplicated according to a symmetrical self-similar scheme. Left: geometry at rest. Right: motion of the structure and definition of the effective degrees of freedom ϕ_n for $n \in 1, N+1$.

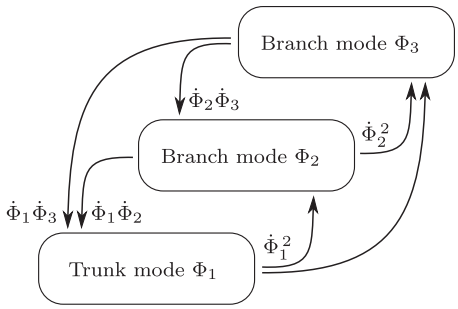

Fig. 12. Nonlinear couplings between effective degrees of freedom for a structure with $N = 2$ levels of branching. Arrows denote energy transfers between modes. All upcoming arrows originating at a given level n are associated with the same variable $\dot{\Phi}_n^2$.

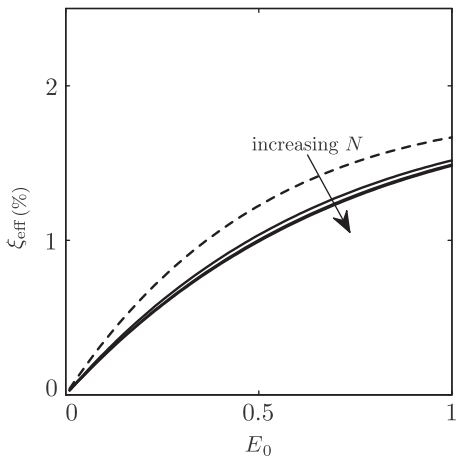

Fig. 13. Effective damping in a self-similar multiply branched symmetrical structure (Fig. 11) as a function of the initial normalised energy. Solid lines (——): increasing values of the maximum branching order from $N = 2$ up to $N = 4$. Dashed line (– – –): reference case $N = 1$ (Section 2). The parameters values are given by solving Eqs. (C.15)–(C.17) using the reference values $\phi_b = \pi/2$, $\Omega = 2$ and $\Gamma = 0.2$.

5.1. Models

A to-be-damped mode ψ of a main rotational structure with moment of inertia J_s and resonance angular frequency ω_s is schematically represented in Fig. 15. The TMBD consists of the elementary model of Section 2 mounted on the main

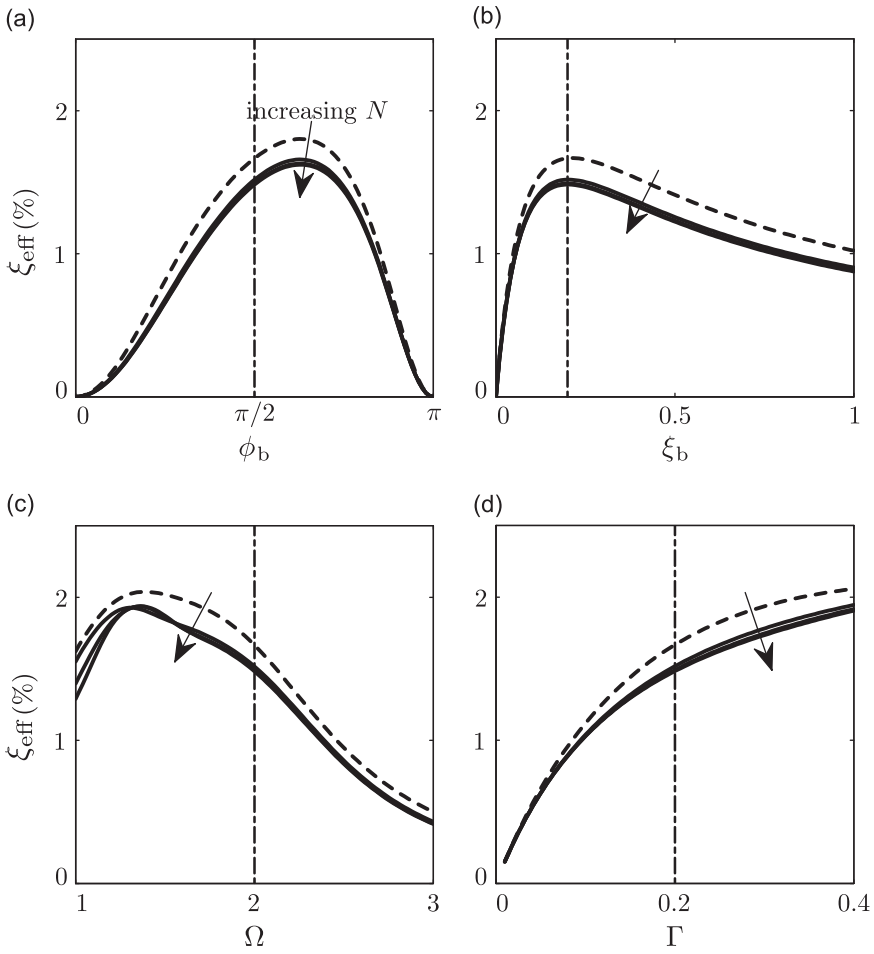

Fig. 14. Dependence of the effective damping ξ_{eff} on the four parameters used for designing the self-similar multiply branched symmetrical structure (see Eqs. (C.15)–(C.17)). The initial normalised energy is $E_0 = 1$. Solid lines (——): increasing values of the maximum branching order from $N = 2$ up to $N = 4$. Dashed line (– – –): reference case $N = 1$ (Section 2). Non-varying parameters are set to the reference values given in Fig. 13 and indicated by a vertical dash-dotted line (–·) in the other diagrams. (a) Effect of the branching angle ϕ_b. (b) Effect of the damping of the branch modes ξ_b. (c) Effect of the ratio Ω between the frequency of the branch mode and that of the trunk mode. (d) Effect of the mass number Γ.

structure with a rotational spring k_t and a damping element c_t in order to damp their relative motion (Fig. 15(a) and (b)). The mass ratio $J = J_\theta/J_s$ is set to 1 percent, a classical value in engineering practice. The parameters of the main structure are defined in reference to those of the branched structure (see Appendix A) with the following normalised motions: $\Psi = \psi/\Lambda$, $\Theta = \theta/\Lambda$, $\Omega_s = \omega_s/\omega_t = \sqrt{J\,k_s/k_t}$.

When the main structure is forced by a moment of amplitude m_0 at a frequency ω_f, the dynamical dimensionless equations are obtained from Eqs. (16) and (1):

$$\ddot{\Psi} + 2J\xi_t\dot{\Psi} + (\Omega_s^2 + J)\Psi = J(\Theta + 2\xi_t\dot{\Theta}) + JM_0\cos(\Omega_s\Omega_f\tau)$$

$$\ddot{\Theta} + 2\xi_t\dot{\Theta} + \Theta = \Psi + 2\xi_t\dot{\Psi} + 2\Gamma\left(\dot{\Theta}\dot{\Phi}\sin(\phi_b + \Phi) - \ddot{\Theta}(\cos(\phi_b + \Phi) - \cos\phi_b\right)$$

$$\ddot{\Phi} + 2\Omega\xi_b\dot{\Phi} + \Omega^2\Phi = -\dot{\Theta}^2\sin(\phi_b + \Phi) \tag{15}$$

Here, the dimensionless parameters are $M_0 = m_0/(k_s\lambda)$, $\Omega_f = \omega_f/\omega_s$ and $\xi_t = c_t/2\sqrt{J_\theta k_t}$.

The TMBD performance needs to be evaluated in comparison to the performance of an equivalent and optimal TMD design. The equivalence on inertia and frequency is achieved with an equivalent TMD being the TMBD with the branches blocked (Fig. 15).

The equivalence on damping is discussed below. For the time being, we simply assume that a given damping element c_{TMD} is put in place of c_t (see Fig. 15). The dynamical reduced equations are

$$\ddot{\Psi} + 2J\xi_{\text{TMD}}\dot{\Psi} + (\Omega_s^2 + J)\Psi = J(\Theta + 2\xi_{\text{TMD}}\dot{\Theta}) + JM_0\cos(\Omega_s\Omega_f\tau)\ddot{\Theta} + 2\xi_{\text{TMD}}\dot{\Theta} + \Theta = \Psi + 2\xi_{\text{TMD}}\dot{\Psi} \tag{16}$$

with $M_0 = m_0/(k_s\Lambda)$, $\Omega_f = \omega_f/\omega_s$ and $\xi_{\text{TMD}} = c_{\text{TMD}}/(2\sqrt{J_\theta k_t})$.

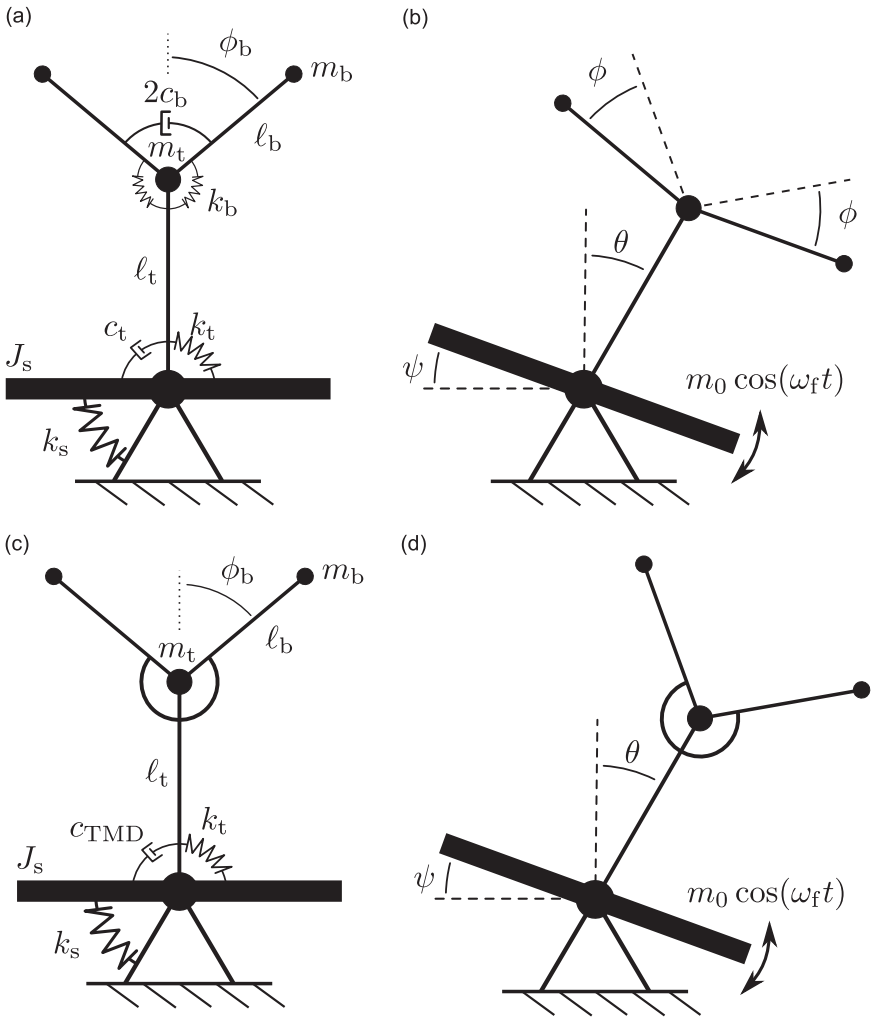

Fig. 15. (a) Geometry and (b) motion of the lumped parameter model of the rotational Tuned Mass Branched Damper (TMBD) coupled to a main undamped structure (see text for symbols). (c) Geometry and (d) motion of the equivalent Tuned Mass Damper (TMD) realised by blocking the branches of the TMBD.

For a given mass ratio J, the optimal values of Ω_s and of the damping ratio ξ_{TMD} are chosen according to the optimisation method described in [15]. The minimal peak frequency response criterion yields $\Omega_s = 1$ and $\xi_{\text{TMD}} = 6$ percent. The equivalence on damping is given by imposing that an equal amount of damping material is used in the TMBD and in the TMD, *i.e.* $c_t + c_b = c_{\text{TMD}}$.

Other choices have to be made on the dimensioning of the branched structure. Somewhat arbitrarily, and after a number of tests on the performance of the TMBD (see below for their characterisation), the amount of dissipative material is equally split between the trunk and the branches: $c_t = c_b$. These two choices on the dissipative material yield

$$\xi_t = \frac{1}{2}\xi_{\text{TMD}} \quad \xi_b = \frac{1}{2}\frac{1}{\Lambda^2 \Omega \Gamma}\xi_{\text{TMD}}. \tag{17}$$

With $\Lambda = \sqrt{1.5}, \phi_b = \pi/2, \Omega = 2$ and $\Gamma = 0.2$ as in Section 2, it comes $\xi_t = 3$ percent and $\xi_b = 5$ percent.

5.2. Results

The performance of the TMBD is compared to that of the TMD by considering the maximum amplitude of the stabilised response to a forced motion. The system equations (16) and (15) are solved numerically in order to obtain the amplitude $\overline{\Psi}$ of the steady state for a forcing moment M_0 at Ω_f. The resonance factor $Q(\Omega_f) = \overline{\Psi}/\Psi_{\text{stat}}$, with $\Psi_{\text{stat}} = M_0 J/\Omega_s^2$, is defined by an extension of the usual resonance factor of a single-degree-of-freedom oscillator. It is displayed in Fig. 16 as a function of the normalised forcing frequency Ω_f for $M_0 = 0.5$. The performance of the damping system can be estimated by the maximum of the resonance factor [15]: $Q_{\max} = \max_{\Omega_f} Q(\Omega_f)$ is found to be about 13 for the TMD and only 11 for the TMBD.

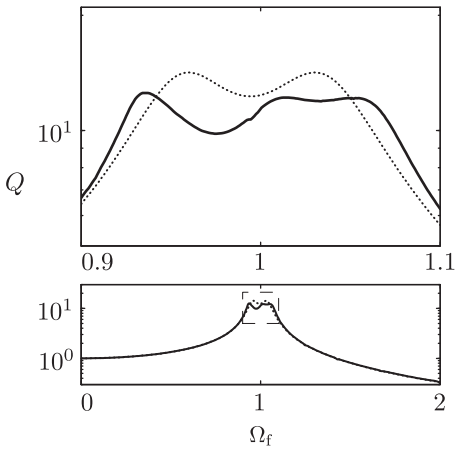

Fig. 16. Resonance factor Q of the main structure as a function of the normalised forcing frequency Ω_f. Dotted line (·····): response of the main structure damped by an optimal TMD, independent of the forcing amplitude. Solid line (——): response of the main structure damped by an equivalent TMBD (see text) for a normalised forcing amplitude $M_0 = 0.5$.

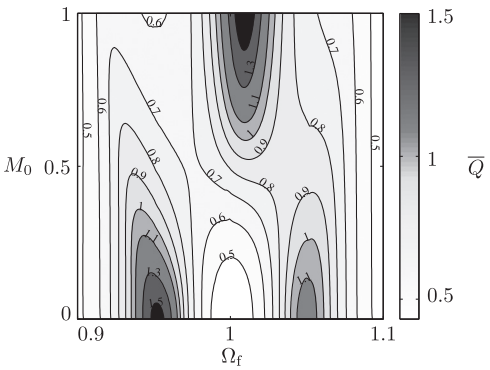

Fig. 17. Map of the steady-state amplitude of the main structure damped by the TMBD, normalised by the performance of the TMD P_{TMD}, as a function of the relative forcing frequency Ω_f and of the normalised forcing amplitude M_0.

The TMBD being nonlinear, it must be compared to the linear TMD for a large range of M_0 (Fig. 17). The TMBD performs better than the TMD for $\overline{Q} = Q_{\mathrm{TMBD}}/Q_{\mathrm{TMD,max}} < 1$.

For low forcing amplitudes ($M_0 < 0.4$), the two peaks correspond to the pattern observed in Fig. 16 and denote a low excitation level of the branch mode. Moreover, since ξ_t is far from the optimal damping ξ_{TMD}, the TMBD brings a lower damping performance than the TMD for this range of amplitude. For high forcing amplitudes ($M_0 > 0.6$), a single peak appears at $\Omega_f = 1$, denoting again a lower damping performance than the TMD. This behaviour is similar to that of a TMD having a larger damping ratio than the optimal value [15]. In-between ($0.4 < M_0 < 0.6$), the TMBD performs better than the TMD.

It must be emphasised that the parameters of the TMBD have been chosen somewhat arbitrarily and might be optimised. However, contrary to the TMD, it seems difficult to approach this question by analytical means.

6. Concluding remarks

A first and important result of the paper is the experimental evidence of the mechanism of damping by branching that was predicted theoretically in [1]. We have shown in Section 2 that a system with well-tuned flexible branches has an effective damping larger than with rigid branches. Moreover, the magnitude of this additional damping and its dependence on the amplitude of motion were well estimated by the models proposed in [1]. It should be noted that this experimental validation was achieved with a system of flexible beams, much more complex than the elementary system of branched articulated segments analysed in [1]; this confirms the numerical results given in this previous paper whereby the DBB mechanism also exists with flexible branched beams.

Following this validation and going back to simple articulated branched systems and numerical predictions, we have analysed in Section 5 a simple implementation: the Tuned Mass Branched Damper. The aim was to explore not only the possibility of using branched systems as tuned dampers, but, more importantly, to compare its efficiency with that of

classical tuned dampers. The results shown in Figs. 16 and 17 show that, in some region of parameter space, a better efficiency is obtained. Still, the improvement is rather minor.

The results of Section 4 allow to draw a much stronger conclusion on the robustness of the mechanism of damping by branching. The analysis was done by systematically exploring variations of the elementary system of branched articulated segments, using numerical simulations and analytical approaches. We have analysed the effect of the source of dissipation (linear or nonlinear, localised or resulting from distributed interaction with a fluid), as well as the effect of multiple branching. In all those cases, the mechanism of damping by branching was observed. Moreover, the dependence of the added damping with the amplitude of motion was always found to be qualitatively similar to that of the generic case described in [1] and recalled in Section 2. Multiple branching was not found to enhance damping by branching, an unexpected result which could be understood using simple arguments.

Overall, this paper does confirm that damping by branching exists as a very robust mechanism in a large variety of branched systems. Promising developments can be expected, considering the simplicity of the concept.

Acknowledgements

This research was funded by the French Ministry of Defence – DGA (Délégation générale pour l'Armement) – through the PhD scholarship program and the Contract 2009.60.034.00.470.75.11.

Appendix A. Dimensionless quantities for the elementary lumped-element model

The notations and dimensionless quantities in use in this paper are

$$J_\theta = m_1\ell_1^2 + 2m_2(\ell_1^2 + 2\ell_1\ell_2\cos\phi_b + \ell_2^2) \tag{A.1}$$

$$\omega_1^2 = \frac{k_1}{J_\theta};\quad \omega_2^2 = \frac{2k_2}{2m_2\ell_2^2};\quad \Omega = \frac{\omega_2}{\omega_1} \tag{A.2}$$

$$\Lambda = \sqrt{\frac{\ell_2}{\ell_1}};\quad \Gamma = \frac{2m_2\ell_2^2}{J_\theta}\frac{1}{\Lambda^2};\quad \xi_b = \frac{c_b}{2\sqrt{k_2 m_2 l_2^2}} \tag{A.3}$$

$$\tau = \omega_1 t;\quad \Theta(\tau) = \frac{\theta(t)}{\Lambda};\quad \Phi(\tau) = \phi(t) \tag{A.4}$$

Appendix B. Dynamical equations and dimensionless quantities in the case of aerodynamical damping

The dimensional equations of motion are those of the elementary model established in [1] with added torques due to the fluid drag:

$$J_\theta\ddot\theta + k_1\theta = 4m_2\ell_1\ell_2\left[\dot\theta\dot\phi\sin(\phi_b+\Phi) - \ddot\theta(\phi_b+\Phi) - \cos\phi_b\right] + M_\theta, J_\phi\ddot\phi + 2k_2\phi = -2m_2\ell_1\ell_2\dot\theta^2\sin(\phi_b+\Phi) + M_\phi, \tag{B.1}$$

where $J_\phi = 2m_2\ell_2^2$. The added torque M_θ on the trunk motion is the integral on each beam length of the product of the local force (Eq. (8)) by the distance from the base of the trunk. It reads

$$M_\theta = -\frac{1}{2}\rho_f C_D\left(d_1\dot\theta^{|2|}\frac{\ell_1^4}{4} + d_2\int_0^{\ell_2}\left((\dot\theta S + \dot\phi s)^{|2|} + (\dot\theta S - \dot\phi s)^{|2|}\right)S\,\mathrm{d}s\right), \tag{B.2}$$

where $S = s + \ell_1\cos(\phi_b+\phi)$. Similarly, the added torque M_ϕ on the branches motion is

$$M_\phi = -\frac{1}{2}\rho_f C_D d_2\int_0^{\ell_2}\left((\dot\theta S + \dot\phi s)^{|2|} - (\dot\theta S - \dot\phi s)^{|2|}\right)s\,\mathrm{d}s. \tag{B.3}$$

Using the dimensionless notations of Appendix A and $d = d_2/d_1, x = s/\sqrt{\ell_1\ell_2}, X = \Lambda x + \cos(\phi_b+\phi)$, the dynamical system (B.1) yields Eq. (10).

Appendix C. Dynamical equations of the multibranched structure and dimensionless quantities

The parameters of the self-similar symmetrical branching scheme of the multibranched structure studied in Section 4.3 are adjusted as follows. The mass m_{n+1}, the length l_{n+1} and the stiffness k_{n+1} of the branches of order $n+1$ (formed at the n-th branching level, with $n < N$) are given by

$$\mu_N = \frac{m_{n+1}}{m_n},\quad \lambda_N = \frac{\ell_{n+1}}{\ell_n}\quad \text{and}\quad \kappa_N = \frac{k_{n+1}}{k_n}\ \forall n \tag{C.1}$$

Table 1
Values of the function $(\pm)_{p,m,k}$ for $p=1$–3.

p	m	$k=1$	$k=2$	$k=3$
1	1	1		
2	1	1	1	
2	2	1	−1	
3	1	1	1	1
3	2	1	1	−1
3	3	1	−1	1
3	4	1	−1	−1

Establishing the dynamical equations is done as for the elementary model. The total kinetic and potential energies are

$$E_c=\frac{1}{2}m_1\ell_1^2\sum_{p=1}^{N+1}\mu_N^{p-1}\sum_{m=1}^{2^{p-1}}v_{p,m}^2 \tag{C.2}$$

$$E_p=\frac{1}{2}k_1\ell_1^2\sum_{p=1}^{N+1}2^{p-1}\kappa_N^{p-1}\,\psi_p^2 \tag{C.3}$$

where $v_{p,m}$ is the velocity of the m-th mass of level p:

$$v_{p,m}^2=\sum_{i=1}^{p}\sum_{j=1}^{p}\lambda_N^{i-1}\lambda_N^{j-1}\left(\sum_{k=1}^{i}(\pm)_{p,m,k}\dot{\psi}_k\right)\left(\sum_{k=1}^{j}(\pm)_{p,m,k}\dot{\psi}_k\right)\cos V_{p,m,i,j}, \tag{C.4}$$

In the above expressions, the angles $V_{p,m,i,j}$ are

$$V_{p,m,i,j}=\sum_{k=1}^{i}\pm_{p,m,k}(\psi_k+\phi_b)-\sum_{k=1}^{j}\pm_{p,m,k}(\psi_k+\phi_b), \tag{C.5}$$

making use of the auxiliary functions $\pm_{p,m,k}=-(-1)^{\lceil m/2^{n-k}\rceil}$ (with $k\le p$), being equal to 1 or -1 depending on the indices p, m and k, and $\lceil x\rceil=\min\{n\in\mathbb{Z}|n\ge x\}$. Table 1 gives the values of $\pm_{p,m,k}$ for $p=1$ to 3.

One defines the inertia J_n which is split into a linear part J_n^{lin} and a nonlinear part J_n^{NL}:

$$J_n=m_1\ell_1^2\sum_{p=n}^{N+1}\mu_N^{p-1}\sum_{i=n}^{p}\lambda_N^{i-1}\sum_{j=n}^{p}\lambda_N^{j-1}\sum_{m=1}^{2^{p-1}}\cos V_{p,m,i,j} \tag{C.6}$$

$$J_n^{\mathrm{lin}}=m_1\ell_1^2\sum_{p=n}^{N+1}\mu_N^{p-1}\sum_{i=n}^{p}\lambda_N^{i-1}\sum_{j=n}^{p}\lambda_N^{j-1}\sum_{m=1}^{2^{p-1}}\cos\left(\sum_{k=1}^{i}\pm_{p,m,k}\phi_b-\sum_{k=1}^{j}\pm_{p,m,k}\phi_b\right) \tag{C.7}$$

$$J_n^{\mathrm{NL}}=J_n-J_n^{\mathrm{lin}} \tag{C.8}$$

Applying the Lagrange equations to the kinetic and potential energies yields (see Appendix C of [13] for a detailed derivation) the following dynamical equations (with linear terms in the right members):

$$J_n^{\mathrm{lin}}\ddot{\psi}_n+2^{n-1}k_1\kappa_N^{n-1}\psi_n=J_n^{\mathrm{NL}}\ddot{\psi}_n+\dot{\psi}_n\left(\sum_{k=n+1}^{N+1}h_{n,k}\dot{\psi}_k\right)+\sum_{k=1}^{n-1}c_{n,k}\dot{\psi}_k^2 \tag{C.9}$$

where the coefficients $h_{n,k}$ and $c_{n,k}$ are given by

$$h_{n,k}=-2m_1\ell_1^2\sum_{p=k}^{N+1}\mu_N^{p-1}\sum_{i=n}^{p}\lambda_N^{i-1}\sum_{j=k}^{p}\lambda_N^{j-1}\sum_{m=1}^{2^{p-1}}\pm_{p,m,k}\sin V_{p,m,i,j} \tag{C.10}$$

$$c_{n,k}=-m_1\ell_1^2\sum_{p=k}^{N+1}\mu_N^{p-1}\sum_{i=n}^{p}\lambda_N^{i-1}\sum_{j=k}^{p}\lambda_N^{j-1}\sum_{m=1}^{2^{p-1}}\pm_{p,m,n}\sin V_{p,m,i,j} \tag{C.11}$$

With the following dimensionless quantities, defined for $n\in[1,N+1]$

$$\omega_n^2=\frac{2^{n-1}k_1\kappa_N^{n-1}}{J_n^{\mathrm{lin}}};\quad \tau=\omega_1 t;\quad C_{n,k}=\frac{c_{n,k}}{J_n^{\mathrm{lin}}} \tag{C.12}$$

$$\Omega_n = \frac{\omega_n}{\omega_1}; \quad \Phi_n(\tau) = \psi_n(t); \quad H_{n,p} = \frac{h_{n,k}}{J_n^{\text{lin}}} \tag{C.13}$$

$$\Upsilon_n = \frac{J_n^{\text{NL}}}{J_n^{\text{lin}}}; \quad \Gamma_n = \frac{J_n^{\text{lin}}}{J_1^{\text{lin}}} \frac{1}{\Lambda^2} \tag{C.14}$$

the dynamics equation (C.9) becomes Eq. (13).

Unfortunately, there is no obvious recurrence relationship between J_n^{lin} and J_{n-1}^{lin} and consequently, neither ω_n nor Ω_n cannot be expressed as simple functions of the same quantities at lower orders.

Choosing the overall branch mass, the frequency ratio Ω_2 between the first branch mode and the trunk mode and the mass ratio Γ_2 pertaining to the first branch level to be the same as the corresponding quantities of the elementary model implies that

$$2\mu_N \frac{(2\mu_N)^N - 1}{2\mu_N - 1} = \frac{1}{\Lambda^4 + \Lambda^2(2\ \cos\ \phi_b - 1/\Gamma) + 1} \tag{C.15}$$

$$\Gamma_2(\lambda_N, \mu_N, \phi_b) = \Gamma \tag{C.16}$$

$$\Omega_2(\kappa_N, \lambda_N, \mu_N, \phi_b) = \Omega \tag{C.17}$$

where Ω, Γ and Λ are defined in Appendix A.

In order to solve this set of equations for μ_N, λ_N and κ_N, we arbitrarily set $\Lambda = \sqrt{0.7}$. One finds μ_N with Eq. (C.15) (setting that the masses of the elementary and of the multibranched structures are the same). The value of λ_N is obtained with Eq. (C.16) and finally κ_N with Eq. (C.17).

References

[1] B. Théckès, E. de Langre, X. Boutillon, Damping by branching: *a bioinspiration from trees*, *Bioinspiration & Biomimetics* 6 (2011) 046010, http://dx.doi.org/10.1088/1748-3182/6/4/046010.

[2] H. Spatz, A. Emanns, O. Speck, The structural basis of oscillation damping in plant stems—biomechanics and biomimetics, *Journal of Bionics Engineering* 1 (3) (2004) 149–158.

[3] R. Blevins, *Flow-induced Vibration*, Van Nostrand Reinhold Co., New York, 1990.

[4] K. Niklas, *Plant Biomechanics: An Engineering Approach to Plant Form and Function*, University of Chicago Press, Chicago, 1992.

[5] F. Brüchert, O. Speck, H. Spatz, Oscillations of plants' stems and their damping: *theory and experimentation*, *Philosophical Transactions of the Royal Society of London, Series B: Biological Sciences* 358 (1437) (2003) 1487.

[6] O. Speck, H. Spatz, Damped oscillations of the giant reed arundo donax (poaceae), *American Journal of Botany* 91 (6) (2004) 789.

[7] H. Spatz, F. Bruchert, J. Pfisterer, Multiple resonance damping or how do trees escape dangerously large oscillations? *American Journal of Botany* 94 (2007) 1603–1611.

[8] J. Moore, D. Maguire, Simulating the dynamic behavior of Douglas-fir trees under applied loads by the finite element method, *Tree Physiology* 28 (1) (2008) 75.

[9] D. Sellier, T. Fourcaud, Crown structure and wood properties: *influence on tree sway and response to high winds*, *American Journal of Botany* 96 (5) (2009) 885.

[10] H.-C. Spatz, B. Théckès, Oscillation damping in trees, *Plant Science* 207 (2013) 66–71.

[11] K. James, N. Haritos, P. Ades, Mechanical stability of trees under dynamic loads, *American Journal of Botany* 93 (10) (2006) 1522.

[12] A. Nayfeh, D. Mook, Nonlinear Oscillations, Wiley Online Library, Weinheim, Vol. 31, 1979.

[13] B. Théckès, Amortissement par le branchement des structures flexibles: une approche bio-inspirée des arbres, PhD Thesis, École Polytechnique, 2012. URL ⟨http://pastel.archives-ouvertes.fr/docs/00/77/77/33/PDF/These_2012.pdf⟩.

[14] M. Païdoussis, S. Price, E. de Langre, Fluid-Structure Interactions: Cross-Flow-Induced Instabilities, Cambridge University Press, New York, 2011.

[15] J. Den Hartog, Mechanical Vibrations, Read Books, Mineola, 2007.